Zhao Bo

College of Textiles,
Zhongyuan University of Technology,
N0. 41 Zhongyuan Road, Zhengzhou, Henan 450007,
People's Republic of China
E-mail: zhaobohenan@sina.com
or zhaobohenan@163.com

Experimental and Numerical Simulation Study of an Air drawing Model of Polyethylene Terephthalate (PET) Polymer and Model of Air Jet Flow Field in the Spunbonding Nonwoven Process

Abstract
An air drawing model of polyethylene terephthalate (PET) polymer and one of the air jet flow field in the spunbonding process are established. The air jet flow field model is solved and simulated by means of the finite difference method. Numerical simulation computation results of the distributions of air velocity match quite well with the experimental data. The air drawing model of the polymer is solved with the help of distributions of air velocity measured by Particle Image Velocimetry. The model's predictions of filament fiber diameters, crystallinities and birefringences coincide well with the experimental data. Therefore it can be concluded that a higher initial air temperature can yield finer filament fiber diameter, and a higher initial air velocity can produce a finer fiber diameter as well. The experimental results show that the agreement between the results and experimental data is much better, which verifies the reliability of these models. Also they reveal great prospects for this work in the field of the computer assisted design (CAD) of the spunbonding process.

Key words: *spunbonding, polyethylene terephthalate, air drawing model, air jet flow field, polymer, fiber diameter, crystallinity, birefringence, drawing, numerical computation.*

Introduction

Spunbonding technology is an important single-step process in which high velocity cool air blows a molten thermoplastic polymer from an extruder die tip, which is then rapidly attenuated into filament fibre and finally polymer resin is converted into a nonwoven web [1 - 4]. The spunbonding web is ideally suited for medical, roof and hygienic materials [5 - 7], and so on. The fibre diameter is strongly affected by the air jet flow field developed by the spunbonding attenuator. To achieve the best web performance, therefore, most researches on the spunbonding process are focused on the effect of process parameters on the fibre diameter and structures of spunbonding equipment. These studies can help better understand technology of the spunbonding process. However, research is seldom conducted on an air drawing model of polymer and model of the air jet flow field in the spunbonding process, which is of great importance. At the same time, as far as the author knows, there are some reports in open literature regarding an air drawing model of spunbonding polymer. However, these reports are only simple introductions. In fact, the fibre diameter is strongly affected by the air drawing model of polyethylene terephthalate (PET) polymer and the model of the air jet flow field. Moreover there is not any literature regarding the study of an air drawing model of polymer nor model of the air jet flow field, which strongly affects the fibre diameter and web performance of spunbond nonwoven. In this paper, an air drawing model of polymer will be established, based on the numerical computational method, comparing numerical results with experimental data obtained with our university equipment.

We established an air drawing model of polymer in the spunbonding process based on numerical simulation computation results of the air jet flow field. The finite difference method was applied to simulate the air jet flow field. Meanwhile we also consider the effects of variation in polymer processes and further study the effects of spunbonding process parameters on the fibre diameter. The final fibre diameters, crystallinities and birefringences predicted show good agreement with experimental data. We also investigated the effects of process parameters such as the initial air velocity on fibre diameter and verify the model's reliability for these relationships.

It is found that the model developed can be applied to predict the drawing effects successfully. The results obtained present great prospects for this research in the field of computer assisted design of the spunbonding process, technology and equipment.

Nomenclature

Q = *polymer mass flow rate, kg/s*
D = *filament fibre diameter, mm*
V = *filament fibre velocity, m/s*
u = *air velocity, m/s*
g = *gravitational acceleration, g/s²*
C_{pf} = *specific heat capacity of melt, J/(kg·K)*
h = *convective heat transfer coefficient, W/(m²·K)*
T = *polymer temperature, °C,*
Ta = *air temperature, °C*
j = *sign carrier of the air drag force, when j is -1 for u > V, and 1 for u < V.*

Greek Symbols

ρ_f = polymer density, kg/m³
ρ = air density, kg/m³
η = shear viscosity of air, Pa·s.

Air drawing theoretical model of spunbonding polyethylene terephthalate polymer

The air drawing model of spunbonding polymer consists of continuity, momentum, energy, and constitutive equations [7 - 16]. The surrounding air conditions (velocity and temperature) are considered as given functions of axial position [17 - 19] and obtained by numerical simulation. Almost all experimental data are well fitted by drag force correlation of the following forms:

Continuity equation

$$Q = \frac{\pi}{4} D^2 V \rho_f \tag{1}$$

where: Q - polymer mass flow rate, D - filament fibre diameter, V - filament fibre mean velocity in the spinning direction, and ρ_f - specific density of the polymer, (this quantity depends on temperature).

As the polymer density varies with polymer temperature, the following correlation [20 - 22] is also introduced:

$$\rho_f = 1.356 - (5\times10^{-4} T) \tag{2}$$

where: T - polymer temperature.

Momentum equation

$$\frac{dF_{rheo}}{dx} = \frac{\pi}{2} j\rho C_f \left(V_a - V\right)^2 D + \\ + Q\frac{dV}{dx} - \rho_f \frac{\pi}{4} D^2 g \tag{3}$$

where: F_{rheo} - rheological force, x - spinning axial direction position, ρ - air density, j - sign carrier of air drag force, when j is -1 for $V_a > V$, and +1 for $V_a < V$, ρ_f - polymer density, V - filament fibre velocity, V_a - x-component of air velocity, drag results from friction between the filament fibre and air when the two are moving with different velocities because the high air suction in the chamber results in high axial air velocities, therefore the relative velocity is used in the term instead of the actual velocity of the filament fibre, g is the gravitational acceleration, and C_f - air drawing coefficient of filament fibre as a function of the Reynolds number, C_f - in ***Equation 3*** was given by Matsui [23, 24] with the following correlation:

$$C_f = \beta \cdot (\mathrm{Re_d})^{-n} \tag{4}$$

where: $\mathrm{Re_d}$ - Reynolds number based on the filament fibre diameter, β, n - fitted constants (values of β and n should be 0.37 and 0.61, respectively, as far as the spunbonding process is concerned).

The empirical relationship expression of Reynolds number is as follows:

$$\mathrm{Re_d} = \frac{\rho D\left|\left(V_a - V\right)\right|}{\upsilon_a} \tag{5}$$

where: ρ - density of the air, $(V_a - V)$ - relative velocity between the moving filament fibre and air, and υ_a - kinematic viscosity coefficient of the air.

The force on the filament fibre parallel to the air stream can then be found from the following relation:

$$F_{drag} = \frac{1}{2}\rho(V_a - V)^2 C_f \pi D L_1 \tag{6}$$

where: F_{drag} - air drag force on the filament fibre, ρ - air density, D - filament fibre diameter, L_1 - filament fibre length.

Energy equation

$$\frac{dT}{dx} = -\frac{\pi D h(T - T_a)}{QC_{pf}} + \frac{\Delta H_f dX}{C_{pf} dx} \tag{7}$$

where: T - filament fibre temperature, T_a - air temperature, h - heat transfer coefficient, which will vary with the axial position, C_{pf} - specific heat capacity of the polymer (it varies with temperature at constant pressure), ΔH_f - heat of fusion of the polymer [17], and $\mathrm{Re_d}$ - degree of crystallinity. The first right - hand side term of ***Equation 7*** describes the decrease in temperature due to heat loss by the fibre to the cooling medium and the second term represents the opposite effect that crystallisation has on the temperature due to the release of the latent heat of fusion. The value for the heat transfer coefficient can be calculated from the following relation between Nu and $\mathrm{Re_d}$.

$$\mathrm{Nu} = \gamma(\mathrm{Re_d})^m \tag{8}$$

$$h = \frac{Nu.K_a}{D} \tag{9}$$

Where the Nusselt number Nu [24], $\mathrm{K_a}$ the air heat conduction coefficient, and γ and m are empirical constants of the correlation.

The values of γ and m are 0.42 and 0.334, respectively.

Like the polymer density, the specific heat capacity at constant pressure of the polymer also changes with the polymer temperature. The correlation [20 - 22] is given as follows:

$$C_{pf} = (0.3 + 6\times10^{-4} T)\times 4.182\times10^7 \tag{10}$$

Constitutive equation

As is commonly known, the polymer melt used in the spunbonding process is a kind of non-Newtonian fluid. However, the simplest constitutive equation i.e., the Newtonian fluid relationship is used in this work because research has shown that the temperature dependence on viscosity is the most dominant effect, while the type of constitutive equation is secondary [25, 26]. Therefore for computational simplicity the Newtonian fluid constitutive equation was introduced in our model:

$$F_{rheo} = \frac{\pi}{4} D^2 \eta \frac{dV}{dx} \tag{11}$$

$$\sigma = \frac{F_{rheo}}{\left(\pi D^2 / 4\right)} \tag{12}$$

$$\eta = 48.71\exp[2650/(T + \\ + 273)]\exp[4(X / X_\infty)^2] \tag{13}$$

where: η - shear viscosity of the air.

Crystallisation kinetics equation:

Variation in the degree of crystallinity along the spinline is given by the following equation:

$$\frac{d}{dx}\left(\frac{X}{X_\infty}\right) = \\ = \frac{n_1 k}{V}\left(1 - \frac{X}{X_\infty}\right)\left[\ln\left(1\Big/\left(1 - \frac{X}{X_\infty}\right)\right)\right]^{\frac{n_1 - 1}{n_1}} \tag{14}$$

where: X_∞ - maximum crystallinity [17], X/X_∞ - relative crystallinity, (ratio of the absolute crystallinity over the ultimate crystallinity of the material), n_1 - the avrami index [17], - k -the crystallisation rate [17].

Birefringence equation

$$\Delta n_{am} = C_{op}\sigma \tag{15}$$

$$\Delta n = \left(1 - \frac{X}{X_\infty}\right)\Delta n_{am} + \frac{X}{X_\infty} f_c \Delta_c^0 \tag{16}$$

$$f_a = \Delta n_{am} / \Delta_a^0 \tag{17}$$

where: C_{op} - stress optical coefficient [17, 27, 28], Δ_c^0 - intrinsic amorphous value [17, 27, 28], Δ_c^0 - crystalline birefringence value [17, 27, 28].

Boundary conditions

$$V(0) = V_0,\ F(0) = F_0,\ D(0) = D_0, \\ X(0) = 0,\ T(0) = T_0,\ F_{rheo}(L) = 0 \tag{18}$$

where: L - chamber length, F_0 - initial rheological force of the polymer melt, V_0 - initial velocity of the polymer melt, D_0 - initial diameter of the polymer melt, T_0 - initial temperature of the polymer melt.

The "freezing-point" is defined as the boundary condition. The method used for determining the initial rheological force F_0 is the searching "freezing-point" method, which requires checking whether the fibre diameters before and beyond some "point" along the filament are equal to each other when F_0 is considered to be the sum of the cumulative gravitational and air drawing force acting upon the frozen part of the filament fibre. If the fibre diameters are found to be the same, the "point" is the so-called "freezing-point" and is used in this iteration as the appropriate initial rheological force.

By means of numerical simulations of the air jet flow field, we can determine the distributions of the x-component of air velocity V_a and air temperature T_a along the axial position x. It allows to solve the air drawing model of the polymer using the fourth-order Runge-Kutta method.

Dynamics balance equation

$$F = F_{asp} + F_{grav} - F_{drag} - F_{inter} \quad (19)$$

where: F - force on the filament fibre, F_{asp} - tension exerted by the aerodynamic drawing device, F_{grav} - gravitational force, F_{drag} - air drag on the filament fibre, F_{inter} - inertial force.

Numerical simulation of the mathematical model of the air jet flow field in the spunbonding process

The fibre diameter of spunbonding nonwoven is intensely affected by the air jet flow field of the spunbonding drafting assembly (attenuator), shown in ***Figure 1***. In this paper, we established a model of the air jet flow field to simulate the flow field and we solved it numerically via the finite difference method. Distributions of the centreline x-component of air velocity along the x-axis are demonstrated.

Governing equations

By ignoring the influence of polymer fibres or strands, air jet flow in the drafting assembly (attenuator) will be a classical fluid flow problem. Since the spunbonding air drawing process in the drafting assembly spinning occurs in a very short time, a two-dimensional, steady, viscous turbulent flow of a perfect gas in the absence of body forces is considered. ***Equation 20***, the governing equation, is expressed as follows:

$$div(\rho u\phi - \Gamma_\phi grad\phi) = S_\phi \quad (20)$$

where

$$\phi = \begin{bmatrix} 1 \\ u \\ T \end{bmatrix} \quad \Gamma_\phi = \begin{bmatrix} 0 \\ \mu \\ k/c \end{bmatrix} \quad S_\phi = \begin{bmatrix} 0 \\ -\nabla p + S \\ S_T \end{bmatrix}$$

where: ρ - air density, u - velocity vector, ϕ - the conserved property, Γ_ϕ - diffusion coefficient, S_ϕ - source term for the variable ϕ, T - temperature, μ - dynamic viscosity, k - heat conductivity, c - specific heat of the fluid, p - pressure, S - source term, and S_T - represents the viscosity disssipation rate.

Considering the compressibility of the air, the ideal gas equation is used to close the equation system:

$$p = \rho_a RT \quad (21)$$

where: R - gas constant.

Theoretical model of the air jet flow field in the spunbonding process

The air jet flow field of the spunbonding process is considered as a steady and viscous flow. The flow field is assumed to be two-dimensional. A k-ε model is the most widely used turbulence model in engineering computations and it yields very accurate results in the case of high Reynolds numbers; it is defined as the preferred turbulence model. The air flow field of model consists of the following equations: continuity, momentum, energy, turbulent kinetic energy and turbulent dissipation rate [29 - 31]. In this paper, we adopted the k-ε standard model for computation. Below some details are given.

Values of the constants of the standard k-ε model are $C_{1\varepsilon} = 1.44$, $C_{2\varepsilon} = 1.92$ and $C_u = 0.09$ [32]. The turbulent Prandtl numbers are as follows: $\sigma_k = 1.0$, $\sigma_\varepsilon = 1.3$, $Pr_t = 1.0$ and $\sigma_t = 0.9$ [32], where σ_t, σ_k and σ_ε are Prandtl numbers of turbulence, turbulent kinetic energy and turbulent dissipation rate, respectively.

Continuity equation

$$\frac{\partial(\rho u)}{\partial x} + \frac{\partial(\rho v)}{\partial y} = 0 \quad (22)$$

where: ρ - air density, u - x-component of the air velocity, v - y-component of the air velocity, x - axial position, and y - transversal position.

Momentum equation in x direction

$$\frac{\partial(\rho uu)}{\partial x} + \frac{\partial(\rho uv)}{\partial y} = 2\frac{\partial}{\partial x}(\mu + \mu_t)\frac{\partial u}{\partial x} + \frac{\partial}{\partial y}(\mu + \mu_t)\left(\frac{\partial u}{\partial y} + \frac{\partial v}{\partial x}\right) - \frac{\partial P}{\partial x} + S_u \quad (23)$$

with, $\mu_t = \rho C_u \frac{k^2}{\varepsilon}$

where: P - air pressure, μ - kinematic viscosity of the air, μ_t - turbulent viscosity of the air, C_u - constant of k-ε model, ε - turbulent dissipation rate of air, k - dissipation rate of turbulent kinetic energy of air.

Momentum equation in y direction

$$\frac{\partial(\rho vu)}{\partial x} + \frac{\partial(\rho vv)}{\partial y} = \frac{\partial}{\partial x}(\mu + \mu_t)\left(\frac{\partial u}{\partial y} + \frac{\partial v}{\partial x}\right) + 2\frac{\partial}{\partial y}(\mu + \mu_t)\frac{\partial v}{\partial y} - \frac{\partial P}{\partial y} + S_v \quad (24)$$

Here, $\mu = \upsilon_a \rho$, $\mu_t = \upsilon_t \rho$

where: P - pressure of the air, ρ density of the air, υ_a kinematic viscosity coefficient of the air, υ_t turbulent viscosity coefficient of the air, μ kinematic viscosity of the air, and μ_t the turbulent viscosity of the air.

Energy equation

$$\frac{\partial(\rho uT)}{\partial x} + \frac{\partial(\rho vT)}{\partial y} = \frac{\partial}{\partial x}\left[\left(\mu + \frac{\mu_t}{\sigma_t}\right)\frac{\partial T}{\partial x}\right] + \frac{\partial}{\partial y}\left[\left(\mu + \frac{\mu_t}{\sigma_t}\right)\frac{\partial T}{\partial y}\right] \quad (25)$$

where σ_t - Prandtl number of turbulence.

Turbulent kinetic energy equation

$$\frac{\partial(\rho ku)}{\partial x} + \frac{\partial(\rho kv)}{\partial y} = \frac{\partial}{\partial x}\left[\left(\mu + \frac{\mu_t}{\sigma_k}\right)\frac{\partial k}{\partial x}\right] + \frac{\partial}{\partial y}\left[\left(\mu + \frac{\mu_t}{\sigma_k}\right)\frac{\partial k}{\partial y}\right] + G_k - \rho\varepsilon$$

with,

$$G_k = \frac{\mu_t}{\rho}\left[2\left(\frac{\partial u}{\partial x}\right)^2 + 2\left(\frac{\partial v}{\partial y}\right)^2 + \left(\frac{\partial u}{\partial y} + \frac{\partial v}{\partial x}\right)^2\right] \quad (26)$$

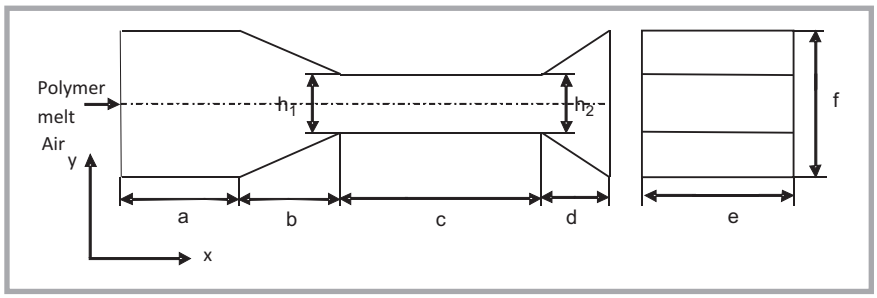

Figure 1. *Flat narrow slot passage of drafting assembly in spunbonding process.*

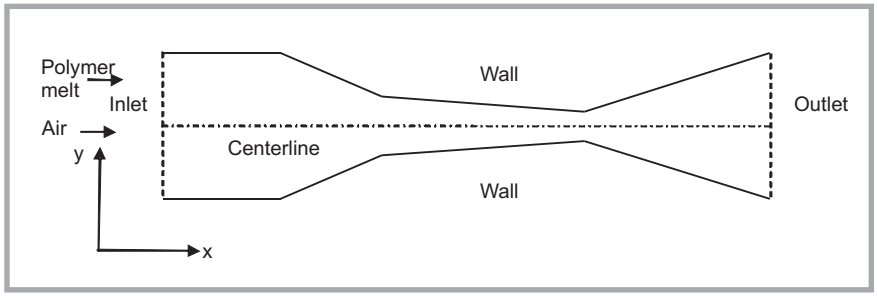

Figure 2. *Computational domain and boundary conditions.*

where: σ_k - Prandtl number of turbulent kinetic energy, σ_t - Prandtl number of turbulence, ε - turbulent dissipation rate of air, k - turbulent kinetic energy of air.

Equation of dissipation rate of turbulent kinetic energy

$$\frac{\partial(\rho\varepsilon u)}{\partial x}+\frac{\partial(\rho\varepsilon v)}{\partial y}= \\ =\frac{\partial}{\partial x}\left[\left(\mu+\frac{\mu_t}{\sigma_\varepsilon}\right)\frac{\partial\varepsilon}{\partial x}\right]+ \\ +\frac{\partial}{\partial y}\left[\left(\mu+\frac{\mu_t}{\sigma_\varepsilon}\right)\frac{\partial\varepsilon}{\partial y}\right]+\frac{C_{1\varepsilon}\varepsilon}{k}G_k-C_{2\varepsilon}\rho\frac{\varepsilon^2}{k} \quad (27)$$

where: σ_ε is the Prandtl number of the dissipation rate of turbulent kinetic energy, $C_{1\varepsilon}$, and $C_{2\varepsilon}$ - constants of the turbulent model, respectively.

Boundary conditions of the air jet flow field model

Figure 2 shows the computational domain and boundary conditions. As the air jet flow field of the spunbonding attenuator is symmetrical along the system's centerline, the plane is chosen as the computation area. The upstream boundary is at the inlet of the spunbonding attenuator. The downstream boundary is considered to be far enough from the inlet of the spunbonding attenuator. The boundaries far enough from the system's centerline are taken as the outer boundaries in the y direction. The following boundary condition correlation is introduced:

1) The conditions of upstream sections with the inlet are

$$u=u_0,\ v=v_0,\ T=T_0,$$

$$k=\frac{3}{2}(u_{avg}I)^2,\ \varepsilon=C_u^{\frac{3}{4}}\frac{k^{\frac{3}{2}}}{l}, \quad (28)$$

$$l=0.07L$$

where: u_0 is the x-component of the initial air velocity, v_0 the y-component of the initial air velocity, T_0 the initial air temperature, C_u = 0.09, u_{avg} average velocity of inlet, I turbulent intensity of the air, and L characteristic dimension of the inlet.

2) The conditions of the wall sections are

$$u=0,\ v=0,\ T=T_W \quad (29)$$

3) The centerline conditions (x direction) are

$$\frac{\partial u}{\partial y}=0,\ \frac{\partial T}{\partial y}=0,\ v=0 \quad (30)$$

4) The conditions of the outer boundaries (y direction) are

$$\frac{\partial u}{\partial x}=\frac{\partial v}{\partial x}=\frac{\partial k}{\partial x}=\frac{\partial\varepsilon}{\partial x}=\frac{\partial T}{\partial x}=0 \quad (31)$$

Numerical methods for solving the air jet flow field model

The air jet flow field model is solved numerically by means of the finite difference method. Below are some details:

a) the SIMPLE algorithm is utilised to solve the problem of the velocity pressure couple;
b) the staggered grid is presented to avoid tooth-like distributions of velocity and pressure;
c) the preferred difference scheme for space independent variables is the second-order upwind difference scheme;
d) the TDMA method is used to solve the difference equations.

The computational domain is rectangular when the coordinate origin is in the centre of the flat narrow slot passage of the drafting assembly. The x-direction is along the spinneret axis. The length (x-direction) and width (y-direction) of the computational domain are 3600 mm and 220 mm, respectively. There are 2700 grids in the x-direction and 600 grids in the y-direction.

Comparison of theoretical results with experimental data

Experiments were carried out on the air jet flow field of the spunbonding attenuator, shown in ***Figure 1***. In order to verify the air jet flow field model, we measured and predicted the effects of spunbonding process parameters on the fibre diameter. Particle Image Velocimetry (PIV-2100), produced by Denmark Dantec Inc., was utilized to measure the air velocity. In the application of PIV-2100, the air was seeded with oil soot (lampblack) aerosol particles in order for the laser light to be scattered and measured. Experiments were carried out on the flow field of the spunbonding drafting assembly.

The flat narrow slot passage of the drafting assembly is shown in ***Figure 1***. The drafting assembly parameters are as follows: the steady flow segment length a = 40 cm, the jet orifice length b = 10 cm, the drafting segment length c = 27.5 cm, the outlet orifice length d = 10 cm, the drafting segment width e = 30 cm, the jet orifice height f = 6 cm, and the drafting segment hight h_1/h_2 = 3.333/2.333 cm. The initial air velocity is 15 m/s. The initial air temperature, 10.2 °C is unaltered in the measurements.

The distribution of the centreline x-component of air velocity along the x-axis is demonstrated in ***Figure 3***, where the experiment data are represented by dots. It was found that the theoretical (numerical) results obtained with the model considered match well with the experimental data.

Numerical simulation of the air drawing model of polymer in the spunbonding process

Experiments were performed on the spunbonding process at our university. A spunbonding attenuator was used for numerical simulation in this study. The parameters of the spunbonding attenuator are as follows: steady flow segment length a = 14.271 cm, the jet orifice length b = 13.229 cm, the drafting segment length c = 203.0 cm, the outlet orifice length d = 129.5 cm, drafting segment width e = 320 cm, jet orifice height f = 22 cm, drafting segment height h1/h2 = 5.666/3.866 cm, and the spinneret hole diameter is 0.045 cm.

The spunbonding process parameters here are the polymer throughput rate, initial (primary) temperature of polymer melt, primary air temperature, primary air velocity, air suction speed, web basis weight, quench pressure, and the venturi gap. The variation ranges of the parameters are 0.15 - 0.55 g/min/hole, 270 - 340 °C, 12.4 - 28.4 °C, 65 - 105 m/s, 2200 - 2600 r.p.m, 18.5 - 33.5 g/m^2, 190 - 290 Pa, and 10 - 30 mm, respectively. The polymer used in the experimental runs was L1482 polyethylene terephthalate (PET) pellet with a melt flow index (MFI) of 78. To condense the discussions and comparisons, a group of fundamental parameters is set up during computations, which includes a polymer throughput rate of 0.20 g/min/hole, initial temperature of the polymer melt of 295 °C, initial air temperature of 15.6 °C, initial air speed of 85 m/s, air suction speed of 2400 r.p.m, web basis weight of 27.5 g/m^2, quench pressure of 240 Pa, and venturi gap of 20 mm. When one processing parameter was varied, the other fundamental values were kept fixed. In the measurement of the fibre diameter, the image analysis method was employed. Images of nonwoven samples were acquired with a Questar three-dimensional video frequency microscope with an enlargement factor of 600 and depth of focus of 1 mm and then processed with Image-Pro Plus image analysis software to measure the fibre diameter. The mean value of the diameters of 200 randomly chosen fibres was considered as the fibre diameter of a polyethylene terephthalate (PET) nonwoven sample. All the samples tested were conditioned for 24 hours at 65% RH and 20 ± 5 °C before evaluation.

The melt flow index (MFI) experiments of polyethylene terephthalate (PET) were performed at a temperature of 270 °C, load capacity 2.160 kg, aperture of the capillary tube 2.095 mm and length thereof 8 mm on the RL-11B melt flow indexer at ambient room temperature conditions.

As we can see from ***Tables 1*** and ***2***, the values measured coincide well with the numerical computation results, which proves the reliability and accuracy of the air drawing model of polymer in the spunbonding process established in our study.

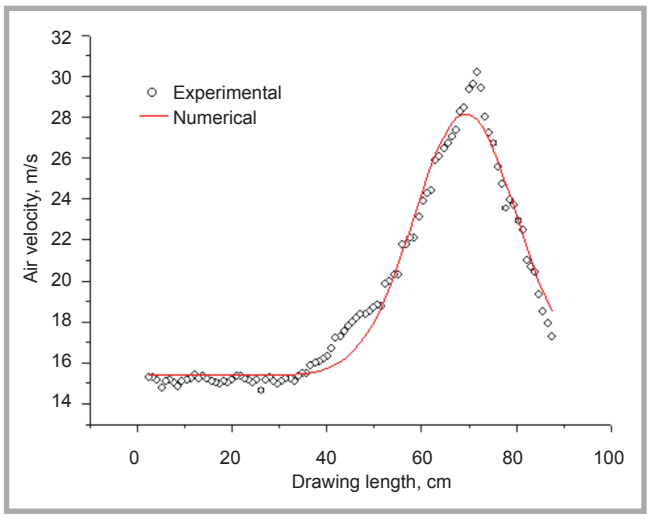

Figure 3. Distributions of centreline x-component of the air velocity along the x-axis.

Effects of spunbonding processing parameters on filament fibre diameter

Effects of the drawing parameters on the fibre diameter can be investigated based on the air drawing model of polyethylene terephthalate (PET). In this work, the effects of the initial air temperature and initial air velocity are investigated. The same spunbonding attenuator is used for numerical simulation in this study. To condense the discussions and comparisons, a group of fundamental parameters is assumed for computations, in which the polymer throughput rate is 0.20 g/min/hole, the initial polymer melt temperature 295 °C, initial air temperature 15.6 °C, and initial air speed 85 m/s.

Relationship between the initial air temperature and fibre diameter

Figure 4.a (see page 94) shows the effect of the initial air temperature on the fibre diameter for the variations changing with distance from the spinneret. The initial air temperature was 12.8 °C, 15.6 °C and 18.4 °C, in turn, from top to bottom. As can be seen, the higher the initial air tem-

Table 1. *Effects of polymer combined parameters (polymer throughput rate and initial polymer melt temperature) on fibre diameter.*

No.	Polymer throughput rate, g/min/hole	Initial polymer melt temperature, °C	Initial air temperature, °C	Initial air speed, m/s	Diameter measured, μm	Diameter predicted, μm	Prediction error, %
1	0.30	295	18.4	75.0	22.78	21.99	3.48
2	0.20				20.11	19.35	3.78
3	0.45				24.17	23.20	4.00
4	0.30	275			25.67	23.20	4.00
5		315			23.52	22.12	5.96

Table 2. *Effects of combined air parameters (initial air temperature and initial air speed) on fibre diameter.*

No.	Polymer throughput rate, g/min/hole	Initial polymer melt temperature, °C	Initial air temperature, °C	Initial air speed, m/s	Diameter measured, μm	Diameter predicted, μm	Prediction error, %
1	0.20	315	15.6	95.0	22.38	21.70	3.06
2			12.8		24.38	23.14	5.09
3			18.4		21.10	20.09	4.80
4			15.6	85.0	25.8	24.40	5.42
5				75.0	22.08	21.11	4.39

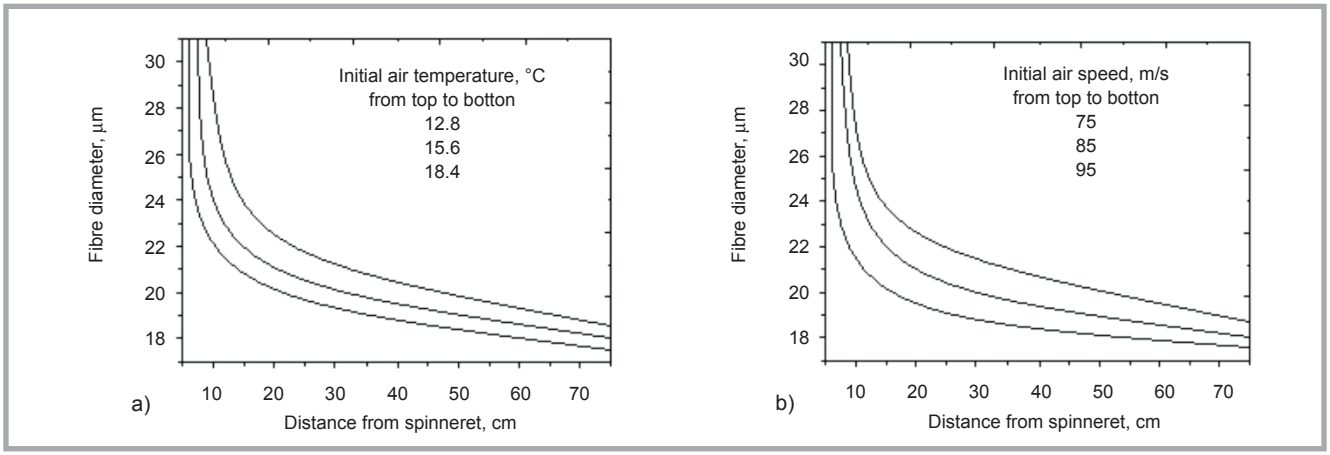

Figure 4. *Showing relationship between fibre diameter and distance from spinneret with initial air: a) temperature, °C and b) speed, m/s.*

perature, the finer the fibre diameter obtained, which is primarily due to the fact that the initial air temperature increased, and both the air drawing force and degree of drawing increased, which yield a finer fibre diameter. Secondly when the initial air temperature increased, the filament fibre cooled more slowly along the spinline, with the drawing (tensile) time of polymer being extended (lengthened), which resulted in a finer fibre diameter. Thirdly when the initial air temperature increased, the viscosity and stress decreased, which produced a finer fibre diameter.

Relationship between the initial air velocity and fibre diameter

Figure 4.b gives the effect of the initial air velocity on fibre diameter, which changes with variations in the distance from the spinneret. Initial air velocities of 75.0 m/s, 85.0 m/s, and 95.0 m/s were considered. As ***Figure 4.b*** shows, the higher the initial air velocities, the finer the fibre diameters obtained, which is mainly attributed to the fact that with an increase in the initial air velocity, air drawing force and degree of drawing, a finer fibre diameter was produced.

Effects of spunbonding nonwoven processing parameters on fibre performance

The subfigures of ***Figure 5*** show the relationship between fibre diameter, polymer melt temperature, fibre crystallinity, fibre birefringence, polymer melt velocity and distance from the spinneret with the polymer throughput rate, as presented by the air drawing model, shown in ***Figure 5***.

Figure 5.a shows the relationship between the fibre diameter and distance from the spinneret with the polymer throughput rate. This figure shows that the fibre diameter decreases more slowly with an increase in the polymer throughput rate. Higher polymer throughput rates also lead to higher fibre diameters, which is primarily due to each polymer throughput rate having its own air speed, with the axial air flow controlling the drag over the entire spinline, which also affects heat loss from the fibre.

Figure 5.b shows the polymer melt temperature profiles for different polymer throughput rates. This figure shows that the cooling rate is lower for higher polymer throughput rates, which is also observed in conventional melt spinning. This is attributed to the fact that the increase in stress is at least partly due to the variations in air flow conditions with a changing polymer throughput rate.

Figure 5.c shows the relationship between fibre crystallinity and the distance from the spinneret with the polymer throughput.

Figure 5.d shows the relationship between fibre birefringence and the distance from the spinneret with the polymer throughput rate. Predictions of fibre birefringence are shown in ***Figure 5.d***, where it is clear that the birefringence is decreasing with an increasing polymer throughput rate. However, at high polymer throughput rates, the curves tend to approach each other down the spinline.

Figure 5.e shows the relationship between the polymer melt velocity and distance from the spinneret with the polymer throughput rate. The polymer melt velocity profiles in ***Figure 5.e*** indicate that the final velocity increases with an increase in the polymer throughput rate, with the velocity tending to stabilise at a higher distance from the spinneret, which is in agreement with the diameter profiles.

Conclusion

An air drawing model of polyethylene terephthalate (PET) polymer and a model of the air jet flow field in the spunbonding process were developed. We numerically simulated the air jet flow field model by means of the finite difference method. Computation results of the distributions of x-components of the air velocity along the spinline during the spunbonding process are in accordance with experimental data as well. The newly developed formulas are introduced into the spunbonding air drawing model to predict the fibre diameter. The distributions of air speed are also introduced into the air drawing model of polyethylene terephthalate (PET) polymer. We can predict the drawing effects by means of the air drawing model, and model predictions of fibre diameters, crystallinities and birefringences are in conformity with experiment data. It was found that a higher initial air speed and a higher initial air temperature can all yield finer fibres. The results predicted coincide well with the actual data measured, which reveal that these models are accurate. It also shows that this area of research has great potential in the field of computer assisted design in the spunbonding nonwoven process and technology.

Acknowledgements

The authors would like to thank Professors Zhen-hua Lu and Ying-zheng Liu of the Turbo machinery Institute at Shanghai Jiaotong University for assistance in the design and construction of the experimental apparatus. The permission by Phoenics Inc. to use their software with an educational license is gratefully acknowledged.

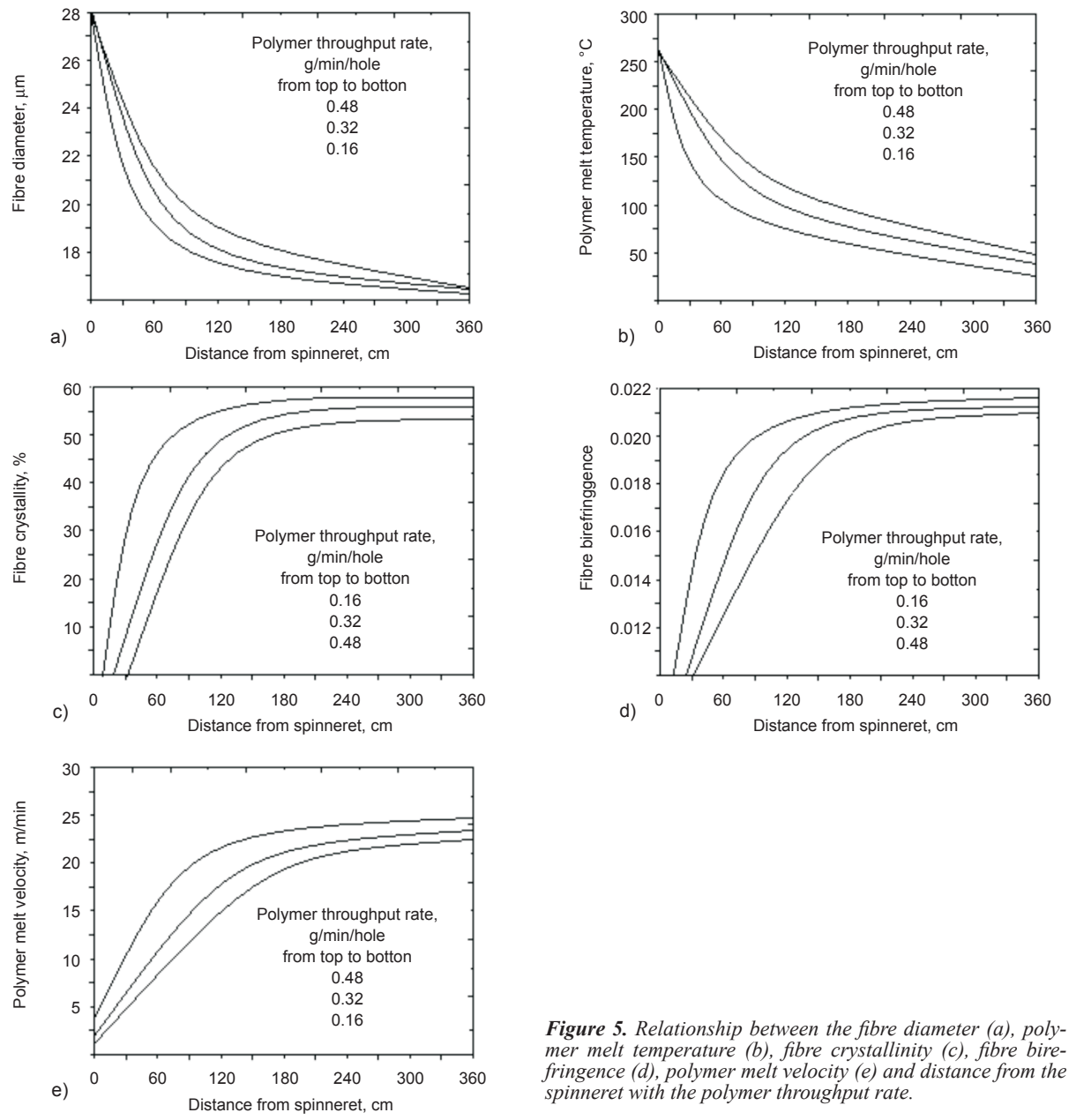

Figure 5. *Relationship between the fibre diameter (a), polymer melt temperature (b), fibre crystallinity (c), fibre birefringence (d), polymer melt velocity (e) and distance from the spinneret with the polymer throughput rate.*

References

1. Malkan SR. An overview of spunbonding and meltblowing technologies. In: *Tappi 1994 Nonwovens Conference* 1994: 31-37.
2. Lu FM. Fundamentals of ason spunbond technology - an innovation to success. In: *Tappi 1998 Nonwovens Conference* 1998: 125-132.
3. Bhat GS, Malkan SR. Extruded continuous filament nonwovens: advances in scientific aspects. *Appl. Polym. Sci*. 2002; 83, 3: 572-585.
4. Smorada RL. Spunbonded technology: an historical perspective. *INDA J. Nonwovens Res*. 1991; 3, 4: 26.
5. Malkan SR, Wadsworth L, Davey C. Parametric studies of the recofil spunbonding process. *Int. Nonwovens J*. 1994; 6, 2: 24-50.
6. Chen CH, White JL, Spruiell JE. Dynamics air drag and orientation development in the spunbonding process for nonwoven fabrics. *Textile Res. J.* 1983; 53, 1: 44-51.
7. Beyreuther R, Malbome HJ. Spunbonded nonwovens-linking innovative polymer, technological and textile research. *Melliand Textilber* 1993; 74(4): 287-289.
8. Hajji N, Spruiell JE, Lu FM, Malkan S. Modeling of the reicofil spunbonding process. *INDA J. Nonwovens Res.* 1992; 4, 2: 16-21.
9. Misra S, Spruiell JE, Richeson GC. Investigation of the spunbonding process via mathematical modeling. *INDA J. Nonwovens Res.* 1993; 5, 3: 13-19.
10. Gagon DK, Dean MM. Computer simulation of steady polymer melt spinning. *Polym. Eng. Sci*. 1981; 21, 13: 844-853.
11. Ziabicke A., Kawai H., High-speed fiber spinning science and engineering aspects, John Wiley & Sons, Inc., 1985.
12. Guo DS, Wang WK. Polyester fibers science and engineering, China Textile Press, Beijing, China, 2001.
13. Taehwan O. Studies on melt spinning process of hollow polyethylene terephthalate fibers. *Polym. Eng. Sci*. 2006; 46, 6: 609-616.
14. Cao JN, Kikutani T. Nonisothermal orientation-induced crystallization in melt spinning of polypropylene. *Appl. Polym. Sci*. 1988; 32: 2683-2697.
15. Bhuvanesh YC, Gupta VB. Computer simulation of melt spinning of polypropylene fibers using a stead state model. *Appl. Polym. Sci*. 1995; 58: 663-674.
16. Kikutani T. High speed melt spinning of bicomponent fibers: mechanism of fiber structure development in polyethylene /

polypropylene system. *Appl. Polym. Sci.* 1996; 62: 1913-1924.
17. Smith AC, Roberts WW. Computational modeling of fiber formation in polypropylene spunbonding with crystallization: comparison with experiments. *Int. Nonwovens J.* 1994; 61, 1: 31-41.
18. Jeon BS. Theoretical orientation density function of spunbonded nonwoven fabric. *Textile Res. J.* 2001; 71, 6: 509-513.
19. Miller C. Effect of filament drawdown on aerodynamic drag and heat transfer in fiber spinning. *AIChE J.* 2004; 50, 5: 898-905.
20. Shenoy AV, Nadkarni VM. Using polyethylene terephthalate melt spinning simulation simulation for process optimization. *Textile Res. J.* 1984; 54, 7: 778-783.
21. Taehwan O. Studies on melt spinning process of hollow polyethylene terephthalate fibers. *Polym. Eng. Sci.* 2006; 46, 6: 609-616.
22. Dutta A, Nadkarni VM. Identifying critical process variables in polyethylene terephthalate melt spinning. *Textile Res. J.* 1984; 54, 1: 35-42.
23. Majumdar B, Shambaugh RL. Air drag on filament in the melt blowing process. *J. of Rheology* 1990; 34, 1: 591-601.
24. Mastui M. Air drag on a continuous filament in melt spinning. *Trans. Soc. Rheol.* 1976; 20, 3: 465-473.
25. Abbott LE, White JL. Melt spinning of high density and low density polyethylene fibers, in development of orientation and crystallinity, and mechanical properties of span fiber. *Appl. Polym. Symp.* 1973; 20: 247-268.
26. Bankar VG, Spruiell JE, White JL. Melt spinning dynamics and rheological properties of nylon-6. Appl. Polym. Sci. 1977; 21: 2135-2155.
27. Salem DR. Structure formation in polymeric fibers, Authorized by Carl Hanser Verlag, 2001.
28. Ziabicki A. *Fundamentals of fiber formation*. John Wiley & Sons, Ltd., 1976.
29. Ke QF, Jin XY. *Nonwovens*. Donghua University Press, Shanghai, China, 2004.
30. Wei TY. *Studies on the processing of PET meltblown nonwovens and its air drawing mathematics model*. Master Thesis. Donghua University, Shanghai, China, 2002.
31. Chen T. *Study on the air drawing in melt blowing nonwoven process*. PhD Dissertation, Donghua University, Shanghai, China, 2003.
32. Edinburgh G, Harlow FH. *Computational fluid dynamics*. Pearson Education Limited, 1996.

Received 23.07.2012 Reviewed 11.03.2013